lubricants

MDPI

Article

Controlling the Solid-State Reaction in Fe-MoS_2 Self-Lubricating Composites for Optimized Tribological Properties

Gabriel Araujo De Lima [1], Aloisio Nelmo Klein [2] and Kaline Pagnan Furlan [3,*]

[1] Department of Mechanical Engineering, Federal University of Santa Catarina (UFSC), Florianópolis 88040-900, Brazil; gabriel.araujo207@gmail.com
[2] Materials Laboratory (LabMat), Federal University of Santa Catarina (UFSC), Florianópolis 88040-370, Brazil; a.n.klein@ufsc.br
[3] Integrated Material Systems Group, Institute of Advanced Ceramics, Hamburg University of Technology (TUHH), Denickestraße 15, 21073 Hamburg, Germany
* Correspondence: kaline.furlan@tuhh.de

Abstract: In this work, self-lubricating composites containing MoS_2 and graphite dispersed in an iron matrix were produced by powder metallurgy and sintering. Previous studies demonstrate that MoS_2 reacts with iron matrixes during sintering, making the production of Fe-MoS_2 composites rather difficult. Therefore, this study focused on a potential solution to avoid or reduce this reaction, whilst still providing good tribological properties. Our results show that the addition of graphite retards the reaction of MoS_2 with iron and that the combination of MoS_2 + graphite results in composites with an optimized coefficient of friction associated with a low wear rate both in nitrogen and air atmospheres. Through adequate control of the lubricant's particle size, composition, and processing parameters, self-lubricating iron-based composites with a low dry coefficient of friction (0.07) and low wear rate (5×10^{-6} $mm^3 \cdot N^{-1} \cdot m^{-1}$) were achieved.

Keywords: self-lubricating composites; sintering; solid lubricants; tribological properties

Citation: De Lima, G.A.; Klein, A.N.; Furlan, K.P. Controlling the Solid-State Reaction in Fe-MoS_2 Self-Lubricating Composites for Optimized Tribological Properties. *Lubricants* **2022**, *10*, 142. https://doi.org/10.3390/lubricants10070142

Received: 2 June 2022
Accepted: 2 July 2022
Published: 6 July 2022

1. Introduction

Friction is present in every mechanical system and is associated with losses in power, performance, and money [1–3]. According to Holmberg et al. [4], up to 1.4% of the world's gross domestic product could be saved by reducing friction losses. Moreover, the authors estimated that about one-third of the total energy generated by fuel combustion in a car is lost in the form of friction in the engine. When not controlled, friction can also result in failure of parts. Thereby, it is of great interest to research means to decrease the friction and wear rate within such systems.

Lubricants have been used by mankind since ancient times. The role of a lubricant is to build a continuous and adherent film between surfaces in contact, providing a low coefficient of friction and preventing them from coming into direct contact, reducing wear and potential failure. Hydrated calcium sulfate (gypsum) was used by the Egyptians in the third millennium before Christ (B.C.) to facilitate the movement and settlement of large blocks of stone [5]. Nowadays, oils and greases are widely used as lubricants worldwide. Unfortunately, oils and greases cannot provide proper lubrication when operating at extreme environmental conditions such as high or cryogenic temperatures, vacuum, radiation, and extreme contact pressure [6–11]. This limits their application in chemical industries, aerospace, cryogenic, or radioactive environments [12]. Under such conditions, the use of solid lubricants is justified and recommended. The incorporation of solid lubricants into mechanical components can be performed using several different techniques including spraying, painting, burnishing, and rubbing. They can also be present

in forms of coatings, deposited via physical or chemical vapor deposition [6]. However, the use of solid lubricants in the form of coatings is linked to a limited life span as the amount of solid lubricant available for lubrication is defined by the film's thickness.

Alternatively, dry self-lubricating bulk composites produced via powder metallurgy (PM) provide a solid lubricant stock for self-replenishment that is virtually infinite, i.e., the solid lubricant is dispersed homogeneously in the whole component. Self-lubricating metallic composites produced via powder metallurgy have been commercially consolidated for many decades and find applications in automobiles, home appliances, electronics, and office and gardening equipment [12,13]. Nevertheless, in the development of PM self-lubricating composites, it is a great challenge to predict the tribological properties resulting from the combination of certain materials based only on the initial powders' (solid lubricants and the matrix) physical, mechanical, and structural properties [6,7,14].

A recent review by our group has shown that the low "thermodynamical stability" of MoS_2 makes the processing of "pure" self-lubricating Me-MoS_2 composites at high temperatures rather difficult [15]. This is especially critical for iron-based matrices, as the iron sulfides present higher stability, i.e., a higher value of (negative) Gibbs free energy of compound formation ΔG^0 than molybdenum disulfide in the range of the temperatures commonly used for the sintering of iron-based composites. This reaction has also been reported by other authors [16–22]. Furthermore, Furlan et al. have shown that for a pure Fe-MoS_2 system the reaction starts already at a very low temperature of 775 °C, altering the microstructural aspects of the lubricant phase [23]. After sintering at 1150 °C, all the MoS_2 is consumed to form FeS in the case of pure iron matrices and mixed sulfides in the case of iron-based matrices containing allowing elements [24].

In a former publication [23], we presented a detailed microstructural analysis of iron-based self-lubricating composites containing only MoS_2, graphite and h-BN sintered at 825 and 1150 °C. Although the composites sintered at 1150 °C showed a clear reaction between MoS_2 or graphite and iron, the samples sintered at low temperatures showed a value of friction coefficient (COF) and wear rate of 0.07–0.10 and 8×10^{-6} mm^3 N^{-1} m^{-1}, respectively. The limiting sintering temperature of 825 °C was higher than the sintering temperature previously reported for the reaction, 775 °C, indicating that the presence of graphite in the initial powder mixture and composite could have a beneficial effect in retarding the consumption of MoS_2 by the solid-state reaction.

In this work, we have studied the influence of the initial graphite particle size, content, and sintering temperature on the reaction between the MoS_2 and the iron matrix. The volume ratio together with the particle size defines the mean free path between the solid lubricant particles and when homogeneously distributed in the matrix, the area that will be lubricated by each particle. Furthermore, we have performed microstructural and tribological characterizations of the sintered composites. Our results confirm that graphite retards the reaction of MoS_2 with the iron matrix, especially when the graphite particles are located around the initial MoS_2 reservoirs and in between the MoS_2 and Fe particles, i.e., for smaller particle sizes. Moreover, there is an optimum graphite amount that assures lubrication without the lubricant's reservoir cover-up during service. With optimized conditions, it was possible to raise the sintering temperature of the composites to 850 °C, whilst achieving a value of COF and wear rate of 0.07 and 5×10^{-6} $mm^3 \cdot N^{-1} \cdot m^{-1}$, respectively.

2. Materials and Methods

Iron, MoS_2, and graphite powders were mixed in a Y-shape mixer for 45 min at different proportions, as listed in Table 1. The powders used in the mix were Fe (Höganäs AB, Höganäs, Sweden, AHC 100.29, d_{50} = 90 μm), MoS_2 (Dow Corning, Midland, TX, USA, Molykote Z, d_{50} = 32 μm), and graphite type a (Nacional de grafite, Itapecerica, Brazil, 99,501, d_{50} = 0.8 μm), type b (Höganäs AB, Höganäs, Sweden, UF4, d_{50} = 5.9 μm), and type c (Nacional de grafite, Itapecerica, Brazil, 99,545, d_{50} = 32 μm). Amide wax, a lubricant usually added to assist in the pressing stage, was not used, since the disulfide acts as a lubricant also in the pressing stage. The optimal volumetric content of 9% for MoS_2 was

defined in a previous study [25]. Cylindrical billets (Ø 20 mm per 6 mm height) were produced by die uniaxial pressing at room temperature and 700 MPa of applied pressure.

Table 1. Powders proportions used in the mixtures.

Sample Name and Description		Composition (vol.%)		
		MoS_2	Graphite	Fe
L_C1a	Fe + C (0.8 μm) + MoS_2	9.0	2.5	Bal.
L_C2a		9.0	5.0	Bal.
L_C3a		9.0	7.5	Bal.
L_C0a		0.0	9.0	Bal.
L_C1b	Fe + C (5.9 μm) + MoS_2	9.0	2.5	Bal.
L_C2b		9.0	5.0	Bal.
L_C3b		9.0	7.5	Bal.
L_C0b		0.0-	9.0	Bal.
L_C1c	Fe + C (32 μm) + MoS_2	9.0	2.5	Bal.
L_C2c		9.0	5.0	Bal.
L_C3c		9.0	7.5	Bal.
L_C0c		0.0	9.0	Bal.

The green samples were sintered in a tubular furnace with resistive heating (Fortelab–FT1200H/3z, São Carlos, Brazil) under a controlled atmosphere of 5% H_2/95% Argon (purity 99.995%) with a constant gas flow of 0.4 L per minute (LPM). During the thermal cycle, a heating rate of 10 °C per minute was used up to the sintering temperatures of 825 or 850 °C with a dwell time of 60 min. A minimum of 3 samples were produced at each sintering condition for each composition.

The density of samples in the green and sintered states were determined by the geometrical method using a precision scale (Mettler Toledo XS205, Greifensee, Switzerland) and a micrometer caliper (Mitutoyo, Kawasaki, Japan). The microstructural morphology of the sintered samples was characterized by optical (Olympus BX60, Tokyo, Japan) and scanning electron microscopy (JEOL JSM-6390LV, Tokyo, Japan) coupled with a detector for chemical analysis via energy-dispersive X-ray spectroscopy (EDS). Prior to such analysis, the samples were metallographically prepared and etched with Nital 2%. Phases characterization and identification were performed by X-ray diffraction measurements (Philips X'pert, Amsterdam, Netherlands, Cu Kα, 40 kV, 30 mA, step size 0.02º, step time 2 s), which were analyzed using the X'Pert Highscore Plus program and the ICDD PDF-2 2004 database. The hardness of the composites was assessed by Vickers microhardness (LECO AMH 43, St. Joseph, MI, USA) in accordance with the MPIF 51 standard using 50 g (HV0.05) of load during 13 s in a total of 5 indentations per sample.

The tribological properties were characterized by unlubricated reciprocating sliding tests (CETR UMT-4, Billerica, MA, USA) under nitrogen (N_2) and air atmosphere at a controlled humidity and temperature. A fixed hard steel sphere (AISI 52100, Só Esferas, São Paulo, Brazil 10 mm Ø) was pressed at a constant load (7 N) against the movable specimen surface (2 Hz, 10 mm stroke) for 60 min (equivalent to 144 m of sliding distance). The wear track volume was measured by optical interferometry (Zygo Newview 7300, Middlefield, OH, USA, 640 × 480 points, 0.28 μm/point, vertical resolution of 0.1 nm) and used to calculate the wear rate. For each composite, a minimum of 3 measurements were performed.

3. Results and Discussion

3.1. Microstructural Analysis

The sintered density of the samples containing graphite and MoS_2 as solid lubricants decreased with the increase in the graphite content (Figure S1) independent of the particle size, which was expected and related to the low density of the graphite (2.26 g/cm^3). Meanwhile, the microstructural phases of the sintered samples differed greatly depending on the graphite content and particle sizes, but also on the sintering temperature (Figure 1). For the smallest particle size (5.9 µm), a homogeneous distribution of the perlite phase is observed, even though the diffusion coefficient of graphite into iron is considered to be smaller at such low sintering temperatures (825 and 850 °C) than at usual sintering temperatures (1150 °C). The perlite phase formation occurs in both the reference samples (Fe + 9% C) as well as the samples with MoS_2.

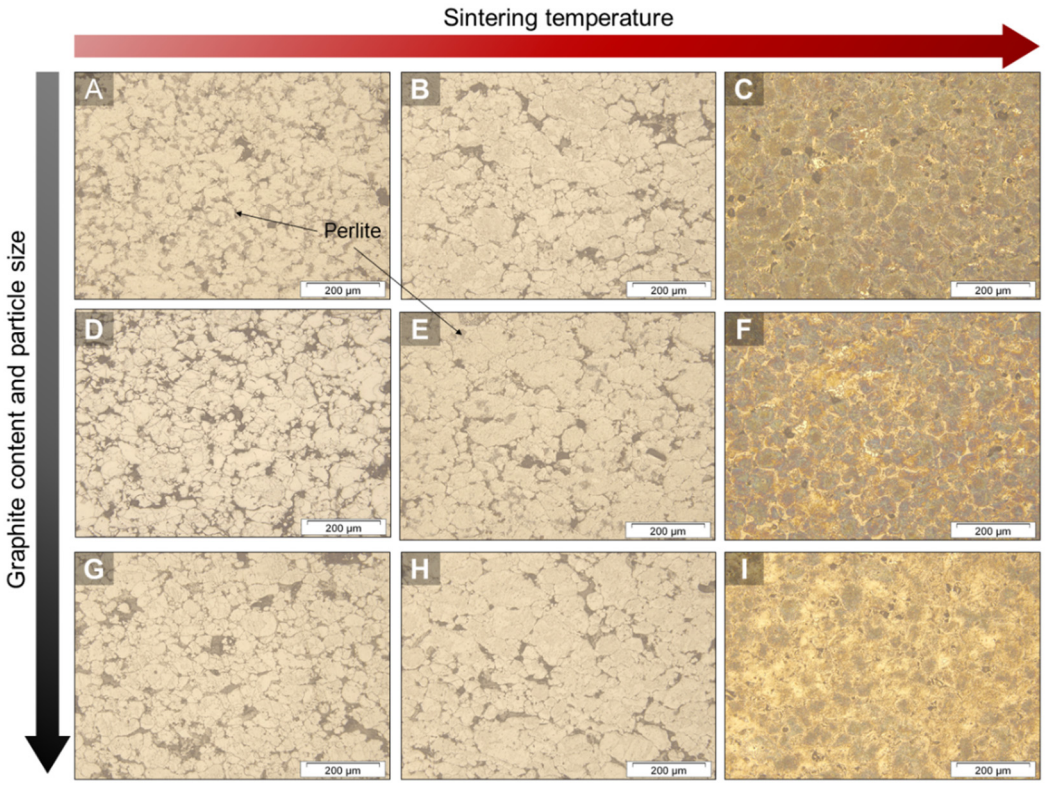

Figure 1. Exemplary microstructures of samples with different particle sizes of graphite (**A**–**C**) 0.8 µm (**D**–**F**) 5.9 µm and (**G**–**I**) 32 µm sintered at low temperatures of (**A**,**D**,**G**) 825 °C and (**B**,**E**,**H**) 850 °C, and (**C**,**F**,**I**) at high temperature of 1150 °C. Samples shown in (**A**,**D**) are the reference samples with Fe + 9% C, whereas the other images are the samples with 9% MoS_2 and (**C**,**F**,**I**) 2.5%, (**B**) 5.0%, and (**E**,**G**,**H**) 7.5% of graphite.

The relevance of the initial particle size of graphite become more evident when analyzing the sintered samples at high temperatures (1150 °C). Although a homogeneous microstructure of fine perlite has been formed for the smaller particle size (0.8 µm), for the largest graphite particle size (32 µm) a non-homogeneous microstructure with ferrite islands between the perlite grains (coarse and fine) is formed. The largest surface area of the smaller particles provides more points of contact during sintering, whilst the reduction of the large free specific surface is a driving force for sintering. This suggests that the carbon content homogenization by diffusion of C into the Fe matrix is achieved after shorter sintering times for smaller particles than for larger particles.

Moreover, the microhardness of the samples' matrixes (indentations made on the matrix) is influenced by the carbon diffusion into the matrix even at such low sintering

temperatures (Figure 2). This leads to an average increase of 56% compared to pure Fe and an average increase of 21% and 17% for 2.5% and 5.0% of graphite, respectively, in relation to the reference sample containing only MoS_2.

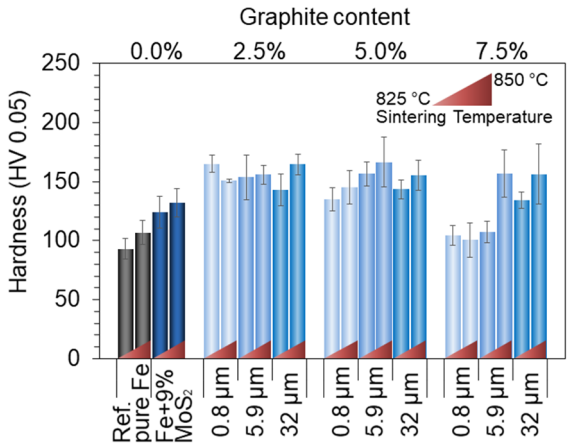

Figure 2. Matrix microhardness of the reference samples and of the samples containing MoS_2 plus different volumetric percentages of graphite sintered at two different temperatures of 825 °C and 850 °C.

In the samples containing MoS_2 and graphite, the increase in the matrix microhardness is caused by two factors: C diffusion in the matrix and Mo and S diffusion from the reaction of MoS_2 with the ferrous matrix. The latter is responsible for the increase in the values between the reference samples of pure Fe and Fe + 9% MoS_2 (0% C). As it will be shown later, the graphite is capable of delaying the MoS_2 consumption in this reaction but it is not able to completely eliminate it. Thus, the low microhardness value found for the matrix with a content of 7.5% C (0.8 µm and 5.9 µm at 825 °C and 0.8 µm at 850 °C) could be associated with the fact that for these samples the carbon prevents the diffusion of Mo and S to the ferritic matrix and therefore the microhardness value remains lower. Note that although the increase in microhardness from the carbon diffusion is desirable, the increase related to the Mo and S diffusion due to the MoS_2 reaction with the matrix is not. Since these mechanisms occur simultaneously, it is difficult to evaluate which graphite content would have the best performance in preventing MoS_2 consumption during the reaction with the matrix by just observing the microhardness results. Moreover, the higher the graphite content, the higher the content of the second phase, which is also known to reduce the hardness [8]. Considering the standard deviations associated with the measurements, it is not possible to observe a clear trend in relation to the initial particle size of graphite in the increase of the matrix microhardness

3.2. Phase Transition and Thermal Stability

The results of a study conducted by Furlan et al. [23], indicated that the addition of graphite had a beneficial effect in delaying the MoS_2 reaction with the ferrous matrix. However, in that previous study, only large contents of graphite (7.5%) and particle size (72 µm) were investigated. It is known that the size of the particles can greatly alter the kinetics of chemical reactions due to the increased surface area [26,27]. Moreover, in sintering practice, the size of the particles within a mix can define and completely alter the particles' distribution within the green body. Although large particles might sit side by side, smaller particles tend to adhere to the bigger particles' surfaces, which in our case, would be the surfaces of the MoS_2 and Fe particles, thus potentially creating an additional barrier to the reaction. Therefore, Table 2 and Figure 3 show the phases formed after sintering of Fe + MoS_2 + Graphite samples according to the initial graphite particle sizes.

Table 2. Identification of phases in the reference samples Fe + 9% MoS_2 and in this composition containing the addition of 5.0% of graphite with different particle sizes sintered at 825 °C and 850 °C.

Sample	Sintering Temperature (°C)	
	825	**850**
Fe + 9% MoS_2	Fe α 06-0696 * MoS_2 37-1492 $FeMo_2S_4$ 71-0379	Fe α 06-0696 $FeMo_2S_4$ 71-0379 $Fe_{1.25}Mo_6S_{7.7}$ 37-1442 FeS 80-1027
Fe + 9% MoS_2 + 5.0% C (0.8 μm)	Fe α 06-0696 Graphite 26-1080 MoS_2 37-1492 $Fe_{1.25}Mo_6S_{7.7}$ 37-1442	
Fe + 9% MoS_2 + 5.0% C (5.9 μm)	Fe α 06-0696 Graphite 26-1080 MoS_2 37-1492 $Fe_{1.25}Mo_6S_{7.7}$ 37-1442	Fe α 06-0696 Graphite 26-1080 MoS_2 37-1492 $Fe_{1.25}Mo_6S_{7.7}$ 37-1442 $FeMo_2S_4$ 71-0379
Fe + 9% MoS_2 + 5.0% C (32 μm)	Fe α 06-0696 Graphite 26-1080 MoS_2 37-1492 $FeMo_2S_4$ 71-0379	

* Numbers indicate the pattern file number according to the database PDF2-2004.

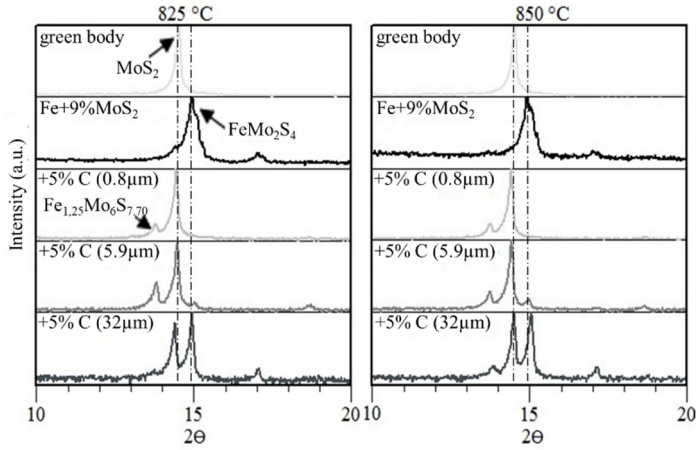

Figure 3. Diffractograms of the reference samples Fe + 9% MoS_2 and of this composition with the addition of 5.0% of graphite with different particle sizes sintered at 825 °C and 850 °C. Zoom in on the regions of interest where the most intense peaks of the sulfides are located. A complete version of the diffractograms with the whole scanned range is found in the Supplementary Information.

The results confirm the effect of graphite in delaying the MoS_2 consumption in the reaction with the ferrous matrix, regardless of the initial particle size. There is no influence of the particle size of the graphite on the temperature for which MoS_2 still exists, but there is a difference between the phases formed, and for the samples containing graphite there is no formation of the FeS phase. In samples containing only MoS_2, the formation of mixed sulfide $FeMo_2S_4$ occurs first, and then the formation of the mixed sulfide $Fe_{1.25}Mo_6S_{7.7}$. This is in agreement with what was reported by Wada et al. [28]. For the graphite with the largest particle size (32 μm), this relation is maintained, whereas for smaller particle sizes (0.8 and 5.9 μm) the preferential formation of the mixed sulfide $Fe_{1.25}Mo_6S_{7.7}$ occurs at 825 °C. Thus, as expected, not only does the addition of graphite influence the formed phases, but also the initial particle size of the graphite.

3.3. Tribological Behavior

The previous results of the study by Furlan et al. [23] pointed out the importance of the matrix hardness in the final tribological behavior, as a too-soft matrix leads to the covering of the lubricant's reservoir and consequent rising of the COF. A graph of the relationship between the coefficient of friction and the wear rate for all samples is shown in Figure 4. The gas atmosphere used in these tests was nitrogen. It is possible to visualize that the higher the coefficient of friction associated with the sample, the greater the wear of the sample. The beneficial effect of adding graphite on the tribological behavior is clearly visualized when comparing it to the reference sample without graphite (black squares), as all the composites investigated here presented values of COF and wear rates lower than the reference sample (Fe + 9%MoS_2) and some samples showed values lower than 0.2 for the COF. Note that these tests were performed in an N_2 atmosphere, which does not favor the lubrication behavior of the graphite [29–31] but highlights the MoS_2 behavior, which then acts as the main solid lubricant. It is also possible to notice the sensible decrease in the composites' wear rates when the sintering temperature is raised by only 25 °C (from 825 °C to 850 °C), which could be associated with the higher matrix hardness discussed earlier (Figure 2).

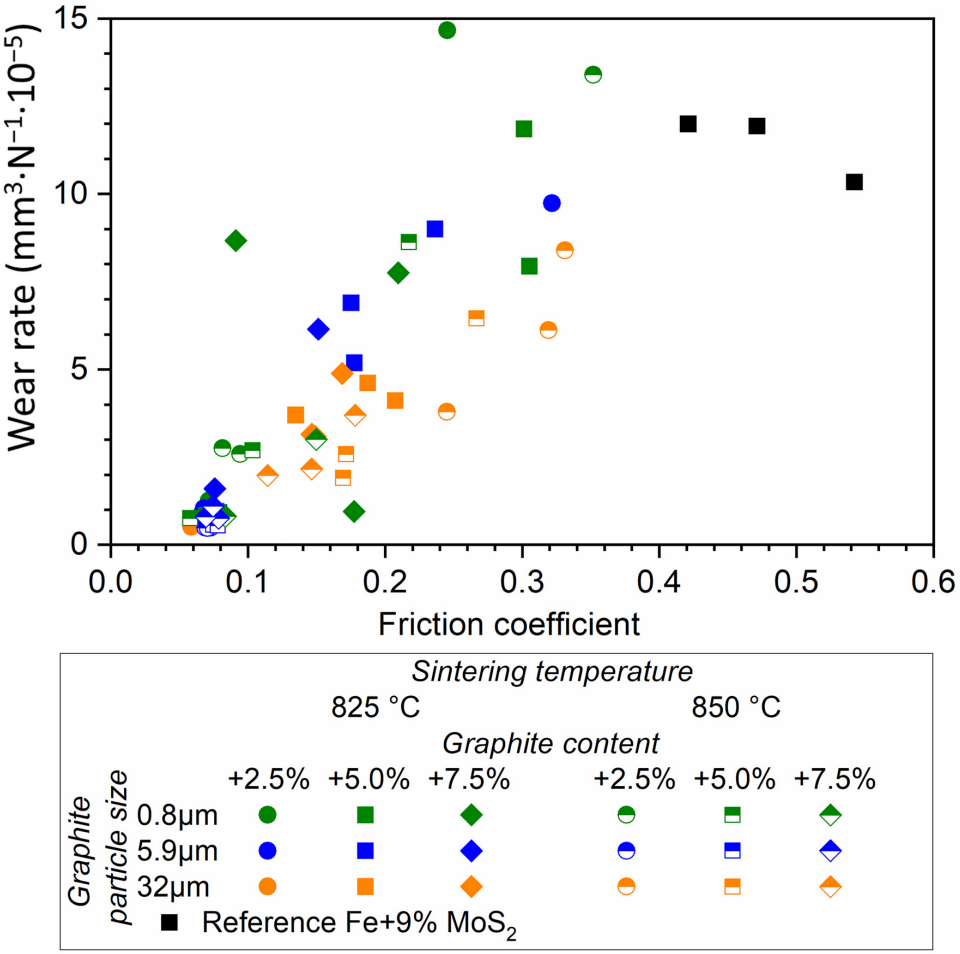

Figure 4. Coefficient of friction vs. wear rate of the samples containing MoS_2 plus graphite sintered at 825 and 850 °C. All the tests were conducted under a nitrogen atmosphere.

Nonetheless, the relation between graphite particle size, content, and sintering temperature does not follow a single trend. At 825 °C, the best performance is that of the sample containing the graphite with the largest particle size (32 µm). This is clear for samples containing 2.5 and 5.0% of graphite, whereas for those containing 7.5% graphite, the sample

with the medium particle size (5.9 µm) shows a smaller COF. At 850 °C, the superiority of this type of graphite (5.9 µm) over the others becomes clear.

Analogously to microhardness, there are two concomitant phenomena with diverse effects: C diffusion into the matrix and MoS_2 consumption due to its reaction with the ferrous matrix, which ends up causing the diffusion of Mo and S into the matrix. Both are favored by the increase in the sintering temperature. Although the dissolution of C, Mo, and S that hardens the matrix may be beneficial, the fact that a greater amount of MoS_2 has been consumed in the reaction is not. Thus, the absence of a trend in the tribological behavior reflects the interactions discussed in the previous sections.

At last, the different graphite powders are manufactured by two different suppliers, which can influence their purity, crystallinity, and porosity [32]. A study published by Pambaguian and Merstallinger [33] showed that the COF and wear rate in Cu matrices containing graphite as a lubricant varied not only according to the content but also according to the type of graphite that was used. Similarly, it is believed that the different types of graphite used here may have diverse properties not only influenced by the particle size, but also by the manufacturing process itself. Unfortunately, the suppliers did not disclose information regarding their fabrication processes.

The performance of the investigated composites is further increased when the test is conducted in air (Figure 5) in which the influence exerted by graphite and the synergistic effect of the two lubricants is favored, as already reported by other authors [29,30,34]. These results point out to the possibility of using these composites in situations where there is a need for lubrication in different atmospheres (vacuum and air, for example). Note the reduced scale of the graph: the coefficient of friction varies between 0.05 and 0.15 and the wear rate between 0 and 20 × 10^{-6} $mm^3 \cdot N^{-1} \cdot m^{-1}$. In this case, the samples containing graphite that showed the best results were the samples with +2.5% graphite of 32 µm particle size sintered at 825 °C and the composites with the initial graphite particle size of 5.9 µm sintered at 850 °C.

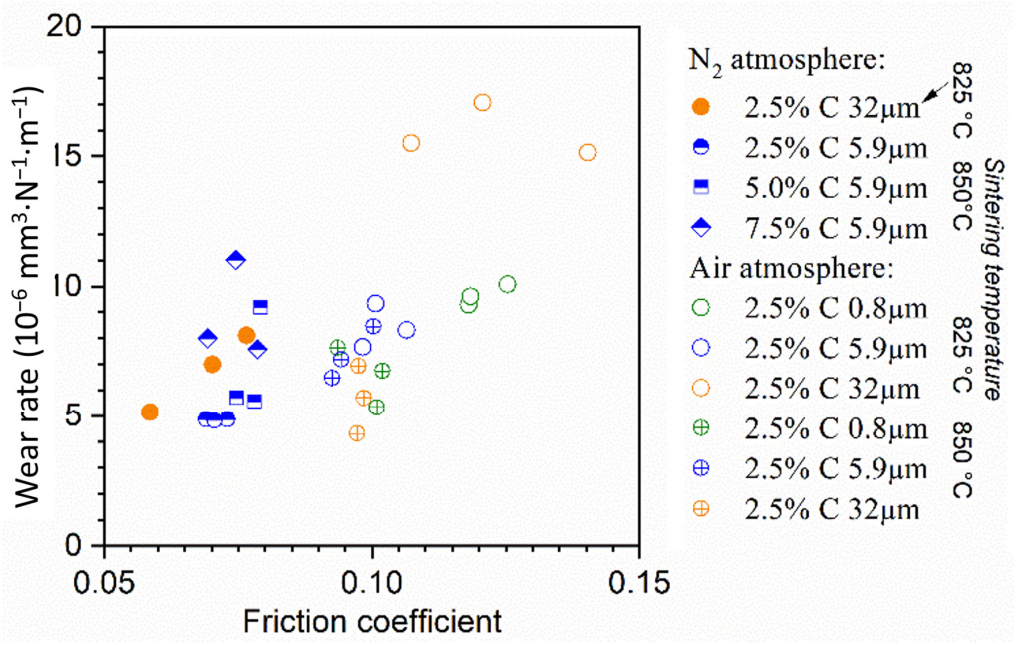

Figure 5. Coefficient of friction vs. wear rate of the composites containing MoS_2 plus graphite tested under nitrogen atmosphere and in air. Zoom in on the regions of interest, i.e., low coefficient of friction (<0.15) and low wear rate (<20 × 10^{-6} $mm^3 \cdot N^{-1} \cdot m^{-1}$).

These results confirm the beneficial effect of graphite in delaying the MoS_2 consumption in the reaction with the iron matrix and the further advantage of the graphite addition for the synergic lubricating behavior, which allowed us to achieve lower values of COF

than previously reported for composites containing MoS_2 in iron-based matrices as well as other metallic matrices (see Table 3).

Table 3. Comparison between the COF of composites reported in the literature and the one obtained in this work. The references are indicated within the table.

Author (Year)	Base Matrix	Composition (w.%)	MoS_2	Graphite	Lowest COF
This work	Fe	Fe	9 vol.%	2.5 to 7.5 vol.%	0.07
Dhanasekaran and Gnanamoorthy (2007) [16]	Fe	Fe + 0.6%C + 2.5%Cu + 3%Ni	3 to 5 w.%	0.0	0.30
Dhanasekaran and Gnanamoorthy (2007) [35]	Fe	Fe + 0.6%C + 2.5%Cu	3 to 5 w.%	0.0	0.30
Li and Xiong (2008) [34]	Ni	Ni + 20%Cr + W + Fe	5, 10 and 15 w.%	3 w.%	0.20
Chen et al. (2012) [29]	Ag	Ag	15 vol.%	5 vol.%	0.14
Chen et al. (2013) [36]	Ag	Ag	0 to 20 vol.%	0 to 20 vol.%	0.12
Huang et al. (2012) [30]	Cu	Cu	0 to 30 w.%	0 to 30 w.%	0.30
Juszczyk et al. (2014) [37]	Cu	Cu + 10%Sn	5 to 20 w.%	5 to 20 w.%	0.20

4. Conclusions

Iron-based self-lubricating composites containing MoS_2 and graphite with a low coefficient of friction and wear rate were fabricated by powder metallurgy and low-temperature sintering. The graphite addition presented a beneficial effect on retarding the MoS_2 reaction with the matrix, that is, the addition of graphite raised the temperature at which all the MoS_2 is consumed to form Fe or Fe-Mo sulfides, which are not lubricants. Moreover, the graphite addition raised the matrix hardness, which also contributed to the good tribological behavior. An interdependent effect between the graphite type, graphite content, and sintering temperature was observed. The best results were achieved by the addition of 2.5% graphite with an initial particle size of 32 µm sintered at 825 °C and 2.5% graphite with an initial particle size of 5.9 µm sintered at 850 °C, which resulted in composites with an average friction coefficient of 0.07 and an average wear rate of 7×10^{-6} $mm^3 \cdot N^{-1} \cdot m^{-1}$ and 5×10^{-6} $mm^3 \cdot N^{-1} \cdot m^{-1}$, respectively. These composites presented a great tribological behavior in both nitrogen and air atmospheres, confirming the synergic effect of both lubricants.

Supplementary Materials: The following supporting information can be downloaded at: https://www.mdpi.com/article/10.3390/lubricants10070142/s1, Figure S1: (A) Density and (B) porosity of the sintered iron samples containing MoS_2 and Graphite as solid lubricants, Figure S2: Diffractograms of the reference samples Fe + 9% MoS_2 and of this composition with the addition of 5.0% of graphite with different particle sizes sintered at 825 °C and 850 °C.

Author Contributions: Conceptualization, methodology, formal analysis, K.P.F.; investigation, data curation, G.A.D.L. and K.P.F.; writing—original draft preparation, G.A.D.L.; writing—review and editing, K.P.F.; supervision and funding acquisition, K.P.F. and A.N.K.; resources, A.N.K. All authors have read and agreed to the published version of the manuscript.

Funding: The present work was developed with financial aid from CNPq (Conselho Nacional de Desenvolvimento Científico e Tecnológico—Brazil) Grant number 163569/2014-2, Whirlpool and BNDES. Research supported by LCME-UFSC.

Institutional Review Board Statement: Not applicable.

Informed Consent Statement: Not applicable.

Acknowledgments: The authors would like to thank the LCME-UFSC for technical support during electron microscopy work, as well as Höganäs Brazil and Dow Corning for providing powder samples.

Conflicts of Interest: The authors declare no conflict of interest.

References

1. Lin, W.; Kluzek, M.; Iuster, N.; Shimoni, E.; Kampf, N.; Goldberg, R.; Klein, J. Cartilage-inspired, lipid-based boundary-lubricated hydrogels. *Science* **2020**, *370*, 335–338. [CrossRef] [PubMed]
2. Colas, G.; Saulot, A.; Michel, Y.; Filleter, T.; Merstallinger, A. Experimental Analysis of Friction and Wear of Self-Lubricating Composites Used for Dry Lubrication of Ball Bearing for Space Applications. *Lubricants* **2021**, *9*, 38. [CrossRef]
3. Jamari, J.; Ammarullah, M.I.; Santoso, G.; Sugiharto, S.; Supriyono, T.; Prakoso, A.T.; Basri, H.; van der Heide, E. Computational Contact Pressure Prediction of CoCrMo, SS 316L and Ti_6Al_4V Femoral Head against UHMWPE Acetabular Cup under Gait Cycle. *J. Funct. Biomater.* **2022**, *13*, 64. [CrossRef] [PubMed]
4. Holmberg, K.; Andersson, P.; Erdemir, A. Global energy consumption due to friction in passenger cars. *Tribol. Int.* **2012**, *47*, 221–234. [CrossRef]
5. Miyoshi, K. *Solid lubrication Fundamentals and Applications*, 1st ed.; Taylor & Francis: London, UK, 2001; p. 416.
6. Busch, C. Solid lubrication. In *Lubricants and Lubrication*; Wiley-VCH: Weinheim, Germany, 2006; pp. 694–714.
7. Erdemir, A. Solid lubricants and self-lubricating films. In *Modern Tribology Handbook*; CRC Press: Boca Raton, FL, USA, 2001; Volume 2, pp. 787–818.
8. Lansdown, A.R. *Molybdenum Disulphide Lubrication*; Elsevier: London, UK, 1999; Volume 35, p. 380.
9. Ludema, K.C. *Friction, Wear, Lubrication-a Textbook in Tribology*, 2nd ed.; CRC Press: Boca Raton, FL, USA, 1996; p. 294.
10. Sliney, H.E. Solid lubricants. In *Friction, Lubrication and Wear Technology-Metals Handbook*; Committee, A.I.H., Ed.; ASM International: Almere, The Netherlands, 1993.
11. Stachowiak, G.W.; Batchelor, A.W. *Engineering Tribology*, 2nd ed.; Butterworth-Heinemann: Waltham, MA, USA, 2001; p. 744.
12. Kostornov, A.G.; Fushchich, O.I. Sintered antifriction materials. *Powder Metall. Met. Ceram.* **2007**, *46*, 503–512. [CrossRef]
13. Davis, J.R. *ASM Specialty Handbook: Copper and Copper Alloys*; ASM International: Phoenix, AZ, USA, 2001.
14. Fedorchenko, I.M. Materials for frictions assemblies. In *Powder Metallurgy, Recent Advances*; Arunachalam, V.S., Roman, O.V., Eds.; Aspect: London, UK, 1990.
15. Furlan, K.P.; de Mello, J.D.B.; Klein, A.N. Self-lubricating composites containing MoS_2: A review. *Tribol. Int.* **2018**, *120*, 280–298. [CrossRef]
16. Dhanasekaran, S.; Gnanamoorthy, R. Microstructure, strength and tribological behavior of Fe–C–Cu–Ni sintered steels prepared with MoS_2 addition. *J. Mater. Sci.* **2007**, *42*, 4659–4666. [CrossRef]
17. Maslyuk, V.A. Sintered Composites Based on Stainless Steel. *Powder Metall. Met. Ceram.* **2000**, *39*, 549–553. [CrossRef]
18. Slys, I.G.; Perepelkin, A.V.; Fedorchenko, I.M. Structure and properties of sintered stainless steel containing molybdenum disulfide. *Sov. Powder Metall. Met. Ceram.* **1973**, *12*, 710–714. [CrossRef]
19. Šuštaršič, B.; Kosec, L.; Jenko, M.; Leskovšek, V. Vacuum sintering of water-atomised HSS powders with MoS_2 additions. *Vacuum* **2001**, *61*, 471–477. [CrossRef]
20. Šuštaršič, B.; Kosec, L.; Dolinšek, S.; Podgornik, B. The characteristics of vacuum sintered M3/2 type HSSs with MoS_2 addition. *J. Mater. Process. Technol.* **2003**, *143–144*, 98–104. [CrossRef]
21. Šuštaršič, B.; Kosec, L.; Kosec, M.; Podgornik, B.; Dolinšek, S. The influence of MoS_2 additions on the densification of water-atomized HSS powders. *J. Mater. Process. Technol.* **2006**, *173*, 291–300. [CrossRef]
22. Mahathanabodee, S.; Palathai, T.; Raadnui, S.; Tongsri, R.; Sombatsompop, N. Dry sliding wear behavior of SS316L composites containing h-BN and MoS_2 solid lubricants. *Wear* **2014**, *316*, 37–48. [CrossRef]
23. Furlan, K.P.; da Costa Gonçalves, P.; Consoni, D.R.; Dias, M.V.G.; de Lima, G.A.; de Mello, J.D.B.; Klein, A.N. Metallurgical Aspects of Self-lubricating Composites Containing Graphite and MoS_2. *J. Mater. Eng. Perform.* **2017**, *26*, 1135–1145. [CrossRef]
24. Furlan, K.P.; Prates, P.B.; Andrea dos Santos, T.; Gouvêa Dias, M.V.; Ferreira, H.T.; Rodrigues Neto, J.B.; Klein, A.N. Influence of alloying elements on the sintering thermodynamics, microstructure and properties of Fe–MoS_2 composites. *J. Alloys Compd.* **2015**, *652*, 450–458. [CrossRef]
25. Furlan, K.P. Estudo da Sinterização e Evolução Microestrutural de Misturas de Fe-MoS_2. Master's Thesis, Federal University of Santa Catarina, Florianópolis, Brazil, 2013.
26. Bueno, P.; Pagnan Furlan, K.; Hotza, D.; Janssen, R. High-temperature stable inverse opal photonic crystals via mullite-sol-gel infiltration of direct photonic crystals. *J. Am. Ceram. Soc.* **2019**, *102*, 686–694. [CrossRef]
27. Furlan, K.P.; Larsson, E.; Diaz, A.; Holler, M.; Krekeler, T.; Ritter, M.; Petrov, A.Y.; Eich, M.; Blick, R.; Schneider, G.A.; et al. Photonic materials for high-temperature applications: Synthesis and characterization by X-ray ptychographic tomography. *Appl. Mater. Today* **2018**, *13*, 359–369. [CrossRef]
28. Wada, H.; Onoda, M.; Nozaki, H.; Kawada, I. The phase relations and homogeneity range of the iron chevrel compound $Fe_xMo_6S_{8-y}$. *J. Less Common Met.* **1985**, *113*, 53–63. [CrossRef]

29. Chen, F.; Feng, Y.; Shao, H.; Zhang, X.; Chen, J.; Chen, N. Friction and wear behaviors of Ag/MoS_2/G composite in different atmospheres and at different temperatures. *Tribol. Lett.* **2012**, *47*, 139–148. [CrossRef]
30. Huang, S.; Feng, Y.; Ding, K.; Qian, G.; Liu, H.; Wang, Y. Friction and wear properties of Cu-based self-lubricating composites in air and vacuum conditions. *Acta Metall. Sin. (Engl. Lett.)* **2012**, *25*, 391–400. [CrossRef]
31. Rowe, G.W. Some observations on the frictional behaviour of boron nitride and of graphite. *Wear* **1960**, *3*, 274–285. [CrossRef]
32. GK_GRAPHITE. Graphit Kropfmühl-Graphite Characterisation. Available online: https://www.gk-graphite.com/en/graphite/characterisation/ (accessed on 8 October 2015).
33. Pambaguian, L.; Merstallinger, A. Self-lubricating copper matrix composites with high contents of lubricants. In Proceedings of the World Tribology Congress, Vienna, Austria, 3–7 September 2001.
34. Li, J.L.; Xiong, D.S. Tribological properties of nickel-based self-lubricating composite at elevated temperature and counterface material selection. *Wear* **2008**, *265*, 533–539. [CrossRef]
35. Dhanasekaran, S.; Gnanamoorthy, R. Dry sliding friction and wear characteristics of Fe–C–Cu alloy containing molybdenum di sulphide. *Mater. Des.* **2007**, *28*, 1135–1141. [CrossRef]
36. Chen, F.Y.; Feng, Y.; Shao, H.; Li, B.; Qian, G.; Liu, Y.F.; Zhang, X.B. Tribological behaviour of silver based self-lubricating composite. *Powder Metall.* **2013**, *56*, 397–404. [CrossRef]
37. Juszczyk, B.; Malec, W.; Wierzbicki, Ł.; Kulasa, J.; Malara, S.; Czepelak, M.; Cwolek, B. Tribological properties of copper-based composites with lubricating phase particles. *Arch. Metall. Mater.* **2014**, *59*, 615–620. [CrossRef]